Journal of Materials Chemistry A

Accepted Manuscript

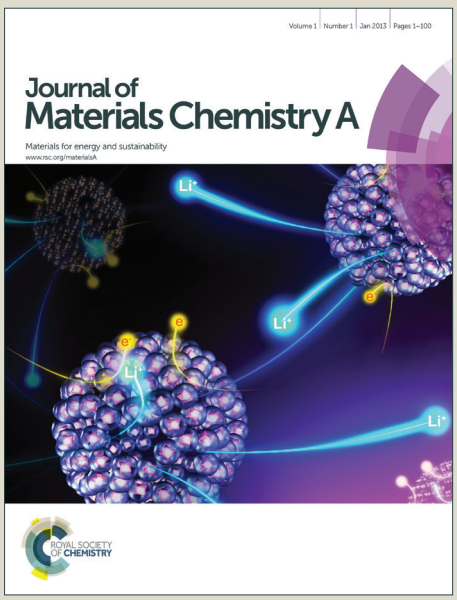

ROYAL SOCIETY OF CHEMISTRY

www.rsc.org/materialsA

Cite this: DOI: 10.1039/c0xx00000x

www.rsc.org/xxxxxx

ARTICLE TYPE

Freestanding three-dimensional graphene and polyaniline nanowire arrays hybrid foams for high-performance flexible and lightweight supercapacitors

Pingping Yu, Xin Zhao, Zilong Huang, Yingzhi Li and Qinghua Zhang

Received (in XXX, XXX) Xth XXXXXXXXX 20XX, Accepted Xth XXXXXXXXX 20XX
DOI: 10.1039/b000000x

Freestanding three-dimensional hierarchical porous reduced graphene oxide foam (RGO-F) was first fabricated by "dipping and dry" method using nickel foam as the template. Three-dimensional (3D) RGO-F with high conductivity provides a large porosity than that of conventional graphene films. Polyaniline (PANI) nanowire arrays aligned on the foam (RGO-F/PANI) were synthesized by in situ polymerization. A symmetric supercapacitor with high energy and power densities was fabricated using RGO-F/PANI electrode. The highly flexible and mechanically foam can directly serve as an electrode with no binders and conductive additives. Owing to its well-ordered porous structure and high electrochemical performance of RGO-F/PANI composite, the symmetric device exhibits high specific capacitance (790 F g^{-1}) and volumetric capacitance (205.4 F cm^{-3}), showing maximum energy density and power density of 17.6 Wh kg^{-1} and 98 kW kg^{-1}. Moreover, the device possesses excellent cycle life with 80% capacitance retention after 5000 cycles.

Introduction

Flexible, lightweight and wearable supercapacitors have attracted great interests in energy storage because of their potential applications in portable electronic devices, flexible displays, electronic paper and mobile phone.[1-3] Supercapacitors show higher energy density than that of conventional capacitor, faster rates of charge/discharge and longer cycle life than that of batteries.[4-8] The freestanding and binder-free electrode with robust mechanical strength and large capacitance is a vital factor for flexible supercapacitors.[9]

Graphene, a two-dimensional monolayer of sp^2-hybridized carbon atoms, has been used as supercapacitor electrode, due to its excellent electrical and mechanical properties, chemical stability, high specific surface area up to 2675 m^2 g^{-1}, and feasibility for large-scale production.[10-12] In current developments, graphene films or papers show the great potential as flexible supercapacitor electrodes with excellent mechanical and electronic properties. However, the aggregation and stacking between individual graphene sheets driven by the strong π-π interaction greatly compromise the intrinsic high specific surface area of graphene. Furthermore, the inefficient ionic and electronic transport in general graphene films has led to capacitance fading over cycling or at high rates, causing a low electrochemical performance of electroactive materials. Therefore, macroscopic graphene framework with three-dimensional interpenetrating structures can solve the issue of poor ionic and electronic transport. Shi et al. prepared a self-assembled graphene hydrogel via a one-step hydrothermal process and deposited reduced graphene oxdied (RGO) hydrogel on the micropores of nickel foam to form a graphene hydrogel/nickel foam composite electrode.[13-14] Choi et al. demonstrated a 3D macroporous structure prepared using polystyrene colloidal particles as sacrificial template.[15] Cheng et al. fabricated a continuous three-dimensional interconnected graphene foam grown by chemical vapour deposition (CVD) on nickel foam.[16] These graphene nanostructures showed well-defined, high conductive and cross linked 3D porous networks with high specific surface area. The 3D porous structure is an ideal scaffold for fabrication of flexible composite electrodes, such as transition metal oxides ($Ni(OH)_2$,[17] Co_3O_4[18] and MnO_2[9]) and conducting polymers[19].

Polyaniline (PANI) is one of the most promising conducting polymers due to its low cost, facile synthesis, and high pseudocapacitance.[20-22] However, the poor stability limits its actual application, owing to the swelling and shrinkage and irreversible degradation of PANI during the charge/discharge process.[23-24] Many studies have incorporated PANI with graphene nanosheets to form hybrid electrode structures, which can provide the synergistic effect of individual constituents on both power and energy densities.[25-29] However, most of these electrodes are papers or films-like based on inter-stacked RGO nanosheets, leading to an inferior ionic accessibility and a modest improvement of the supercapacitor performance. Therefore, design and fabrication a well-defined and highly-ordered continuous porous composites will be a scientific and technical challenge.

In this paper, we report a facile and cheap method to prepare a freestanding and lightweight flexible RGO-F, and then vertically deposit PANI nanowire arrays on the 3D macroporous RGO-F

networks to fabricate RGO-F/PANI composites. Nickel foams (NF) were immersed in the GO suspension, and then RGO-F was obtained by removal of NF and reduction of hydroiodic acid (HI), as shown in Scheme 1. The 3D flexible lightweight RGO-F as skeletons to construct RGO-F/PANI nanostructured hybrid electrodes is the key to our fabrication process. The as-prepared RGO-F with good electrical conductivity owns hierarchical macroporous network structure and high internal surface area. PANI nanowires arrays grown on the RGO-F networks can enhance the specific capacitance and ensure to utilize the porous frameworks of the flexible substrate. The resultant 3D RGO-F/PANI composite architecture retains most of the structural properties of the RGO-F, which facilitates an easy access of the electrolyte ions into the electrodes. The RGO-F/PANI composite electrodes are binder-free, which will reduce the interfacial resistance and enhance the electrochemical reaction rate. The symmetric SC device based on RGO-F/PANI6 electrodes in 1 M H_2SO_4 electrolyte exhibit a specific capacitance of 790 F g^{-1}, a maximum power density and energy density of 98 kW kg^{-1} and 17.6 Wh kg^{-1}, respectively, and a cycling performance of 80 % of initial capacitance over 5000 cycles.

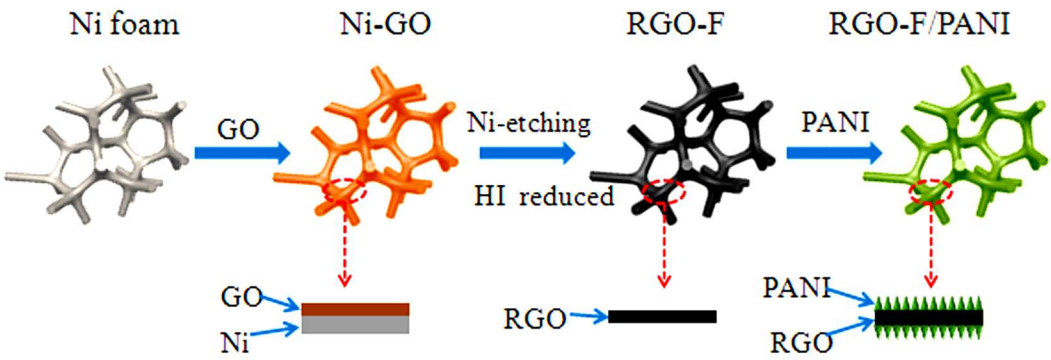

Scheme 1. Schematic illustration of the dip coating process of RGO-F and RGO-F/PANI composites.

2. EXPERIMENTAL SECTION

2.1. Synthesis of 3D RGO-F

3D RGO-F was synthesized by a facile dipping method using NF as the template. GO was prepared by the oxidation of natural graphite powder (180 mesh, Qingdao Tianhe Graphite Co.) according to the modified Hummers' method (see the supporting information for details).[30-31] NF sheets (2 cm × 2cm × 0.1cm, mass per unit area 50.8-53.4 mg cm^{-2}, from Shenzhen Luchuang Environmental Audio Supplies limited Company) were immersed into the GO suspension (5 mg mL^{-1}) for 1h to ensure the GO suspension into the micropores of NFs. The as-prepared NFs with GO suspensions were immersed into hydrochloric acid (3M) at 60 □ for 5 h to remove the NF. After they had cooled to room temperature, the GO foam was washed with deionized water to remove residual acid and metal ions. The GO foam were reduced by the HI heated up to 80 □ for 1h, then washed with a large amount of deionized water, ethanol and isopropanol, finally, dried in an oven at 60 □ for 24 h. The RGO-F was obtained.

2.2. Preparation of RGO-F/PANI

Aniline (AR) was added to 40 mL of 1 M H_2SO_4 aqueous solution, and RGO-F fixed on glass slide (2 × 2 cm^2) were carefully immersed into the above solution without stirring for 3 h to ensure complete adsorption of the aniline. Another 40 mL of 1 M H_2SO_4 aqueous solution containing ammonium peroxydisulfate (APS, AR) was rapidly added and stirred for 1 min. The polymerization was carried out at a temperature of -5 °C. The molar ratio of aniline to APS was 4:1. After reacting overnight, the RGO-F/PANI composites were removed and washed with deionized water several times. A dark green layer formed on the surface of RGO-F. The composites were dried under vacuum at 40 °C for 10 h. A series of RGO-F/PANI electrodes were fabricated from solution with different aniline concentration of 0.03, 0.04, 0.05 and 0.06 M, and the as-prepared RGO-F/PANI composites were termed as RGO-F/PANI3, RGO-F/PANI4, RGO-F/PANI5 and RGO-F/PANI6, respectively. The weight of PANI adsorbed on the RGO-F networks was calculated by the weight difference before and after the polymerization process.

2.3. Structural and morphological characterization.

Field emission scanning electron microscopy (FESEM, Hitachi S-8000) with an X-ray energy dispersive spectroscopy (EDS) was employed to characterize the morphology of the samples. Raman spectra were recorded using a LabRam -1B Ramen spectroscope with He-Ne laser excitation at 632.8 nm and scanning for 50 s. X-ray photoelectron spectroscopic (XPS) measurements were performed on a PHI 5000C ESCA System using a monochromic Al X-ray source (97.9 W, 1486.6 eV), the data analysis was carried out by using the RBD AugerScan 3.21 software provided by RBD Enterprises. The element spectra was chosen (C 1s or N 1s), moved front and back. Each move is less than 7 ev. The curve was subtracted background, and used the "curve fit" to find the corresponding peaks.

2.4. Electrical and electrochemical measurements.

Cyclic voltammetry (CV), electrochemical impedance spectroscopy (EIS), and galvanostatic charge/discharge measurements were conducted on a CHI 660D electrochemical workstation (CH Instruments, Inc., China). An aqueous solution of 1 M H_2SO_4 was used as the electrolyte. The RGO-F, RGO-F/PANI3, RGO-F/PANI4, RGO-F/PANI5 and RGO-F/PANI6 electrodes and separator were wetted with the aqueous electrolyte overnight. The two identical RGO-F or RGO-F/PANI composite electrodes were assembled in a test cell as shown in our previous

report,[32] which consisted of two Pt wires, two electrodes, and separator. The assembly was then encapsulated by a flexible poly (ethylene terephthalate) film.

The specific capacitance of a supercapacitor cell (C_t) is calculated from the equation of $C_t = I\Delta t/m\Delta V$ (1). In symmetric supercapacitors, the specific capacitance (C_{sc}) of the electrodes (RGO-F, RGO-F/PANI composites) is calculated according to $C_{sc} = 4C_t$. The volumetric capacitance (C_{vol}) of electrodes is calculated from the equation of $C_{vol}=C_{sc}\ \rho$ (2), where ρ is the packing density of electrode. The maximum energy density (E) and power density (P) of the symmetric supercapacitors are achieved by the following equations:

$$E = C_{sc}V_{\max}^2 / 8 \quad (3)$$

$$P = (V_{\max} - V_{drop})^2 / (4R_{ESR}m) \quad (4)$$

where I (A) is the discharge current, Δt (s) is the discharge time, m (g) is the total mass of two active electrodes, and ΔV (V) is the potential window during the discharge process. Equivalent series resistance (R_{ESR}) is estimated with the formula $R_{ESR}=V_{drop}/(2I)$, and here V_{drop} (V) is the voltage drop at the beginning of the discharge and I (A) is the constant current.

3. Results and discussion

3.1. Microstructure and morphology

The free standing and lightweight flexible RGO-F was prepared by immersing a piece of NF with a weight of 50.8-53.4 mg cm^{-2} (Figure 1A-a) into GO suspension. By dipping and drying method, NF being coated with GO sheets turns to light yellow. After removed of NF, 3D GO foam is reduced by HI and RGO-F is obtained with a weight of 0.90 - 0.96 mg cm^{-2} and a thickness less than 500 μm (Figure 1A-c). The freestanding 3D RGO-F obtained by this "dipping and dry" way show a superior flexibility as shown in Figure 1B, and a good conductivity (1600 S m^{-1}). Obviously, the resulting graphene network is continuous with topographic features defined by the nickel substrate underneath. Figure 1C shows that the RGO-F replicates the interconnected 3D scaffold structure of the NF template, providing a higher porosity and surface area than that of conventional graphene films.[33-34] The graphene sheets in the RGO-F are in direct contact with each other without obvious breaks. The pore size of RGO-F is about 100 - 300 μm, providing a sufficient space to deposit active materials with uniform penetration into the 3D structure. Furthermore, the ripples and wrinkles in graphene sheets may lead to a better adhesion between RGO-F and conducting polymers or metal oxides to form composite materials. Figure 1D shows the TEM image of a graphene sheet, and the number of layers is 6-8 in our experiment (Figure S1). The selected area electron diffraction (SAED) pattern (inset of Figure 1D) gives reflection spots arranged in a typical hexagonal pattern, indicating the formation of graphene.

The 3D RGO-F with a high conductivity can be used as freestanding flexible electrodes, which is an ideal scaffold for active materials. PANI nanowire arrays were grown on the networks of 3D RGO-F by in situ polymerization. Figure 2A shows a piece of RGO-F/PANI. The uniform dark green color indicates that the PANI is in the proton doped emeraldine salt state which is confirmed by FTIR spectroscopy (Figure S2). Figure 2B and 2E show that the as-prepared RGO-F/PANI5 and RGO-F/PANI6 composites retain the 3D structures and porous morphologies of RGO-F, indicating that the PANI nanowires layer does not change the porous structure of 3D graphene networks. Furthermore, the increasing content of PANI in the composites results a disordered morphology of the composites. At low content of PANI, vertical PANI nanowire arrays are uniformly grown on the skeleton of graphene sheets and maintain their structures to profit from the fast access of ions to electrolytes (Figure 2C and 2D). However, upon increasing the loadings, the PANI nanowires became disordered on the RGO-F (Figure 2F), due to the heterogeneous nucleation process in the heterogeneous deposition process. The TEM images of RGO-F/PANI5 show that an average length of uniformly aligned nanowires is up to approximately 150 nm, as shown in Figure 3A and 3B. In addition, the surface distribution of C, O, and N elements in RGO-F/PANI5 was investigated by energy-dispersive spectroscopy (EDS) mapping. As shown in Figure 3C, a uniform distribution of PANI has been achieved for all of the major constituent elements in the graphene foam.

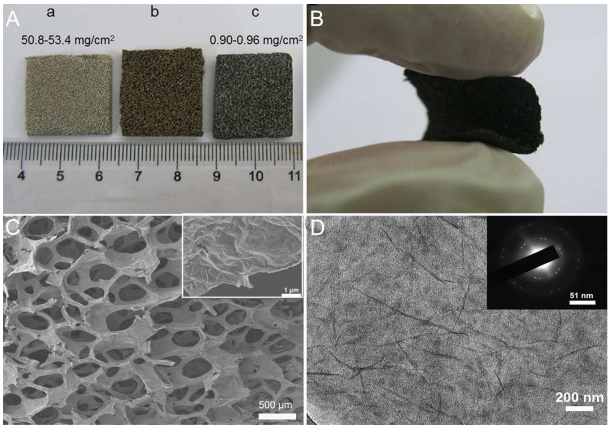

Figure 1. (A) Digital phototgraphs of (a) Ni foam , (b) GO foam with Ni foam and (c) RGO-F; (B) Digital phototgraph of free standing and flexible 3D RGO-F; (C) SEM images of 3D RGO-F, inset showing a high magnification SEM image; (D) TEM image of a graphene nanosheet with its SAED pattern.

Cite this: DOI: 10.1039/c0xx00000x

www.rsc.org/xxxxxx

ARTICLE TYPE

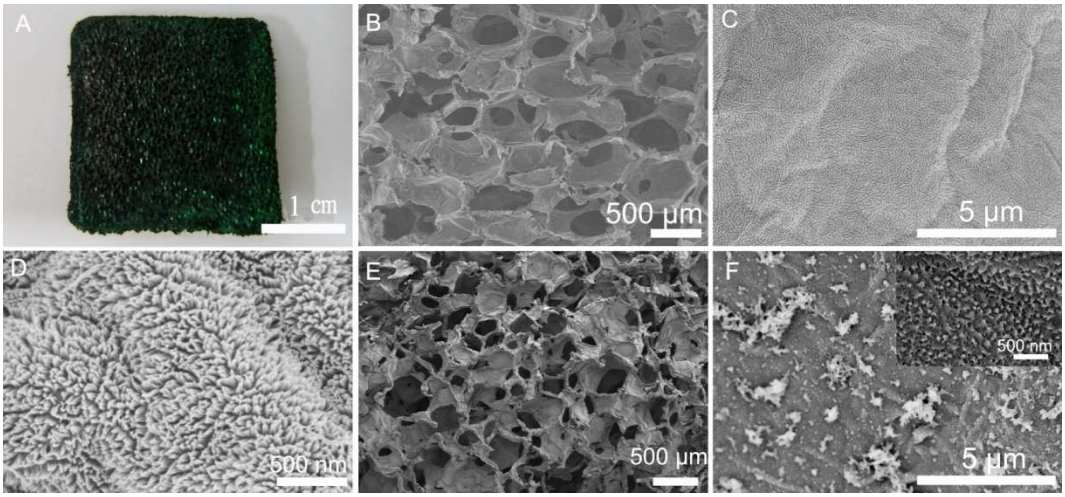

Figure 2. (A) Digital photograph of RGO-F/PANI. (B), (C) and (D) SEM images of RGO-F/PANI5 with different magnification. (E) and (F) SEM images of RGO-F/PANI6 at low and high magnification.

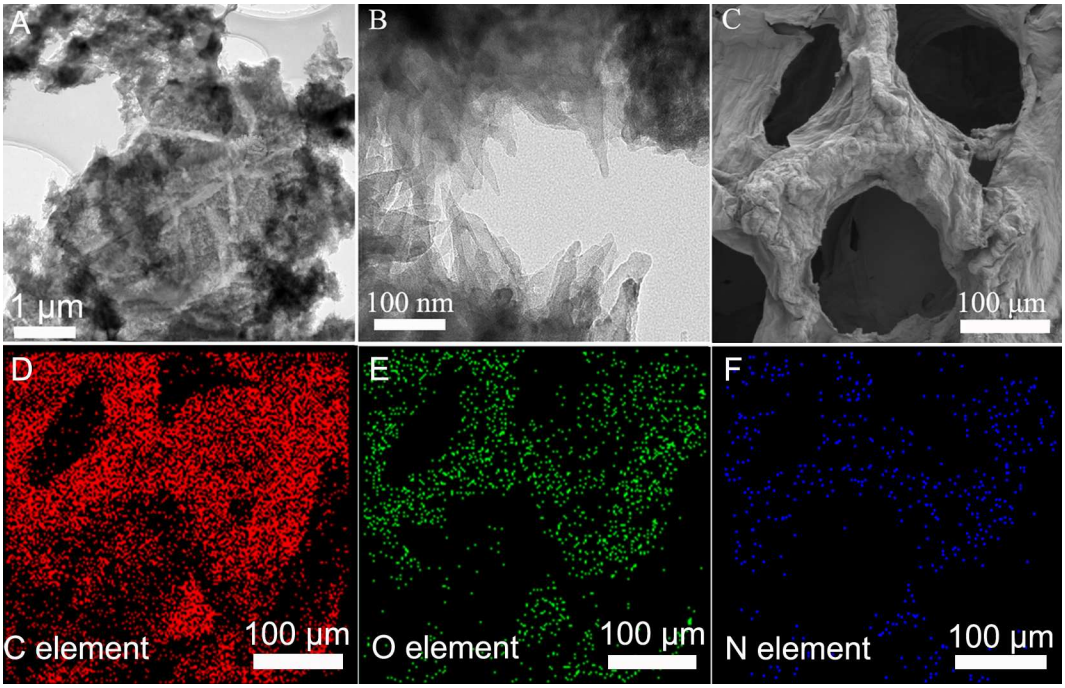

Figure 3. TEM images of RGO-F/PANI5 at low (A) and high (B) magnification. (C) SEM image combined with EDS mapping in the same area and relative intensities of C (red), O (green) and N (blue) elements (D, E and F).

Raman spectra of RGO-F, RGO-F/PANI5 and RGO-F/PANI6 in Figure 4 further confirm the structures of PANI on the RGO-F. There are two prominent peaks at 1340 and 1586 cm^{-1}, corresponding to the D band (C-C, disordered graphite structure) and G band (sp^2 hybridized carbon), respectively.[35] The I_D/I_G ratios are 0.92 for RGO-F and 1.12 for GO (Figure S3), suggesting an increasing order degree after chemical reduction. The peak at ~1620 cm^{-1} (D′) occurs via an intravalley double-resonance process in the presence of defects.[36-37] The RGO-F/PANI5 and RGO-F/PANI6 spectra exhibit the bands in combination with the RGO-F. The bands at 1164, 1253, 1337, 1482 and 1583 cm^{-1} are assigned to C-H bending of the quinoid ring, C-H bending of the benzenoid ring, $C\text{-}N^+$ stretching vibration, C=C vibration of the quinoid rings and C-C srretching of the benzenoid ring, respectively,[38-39] indicating the presence of a conductive PANI structure.

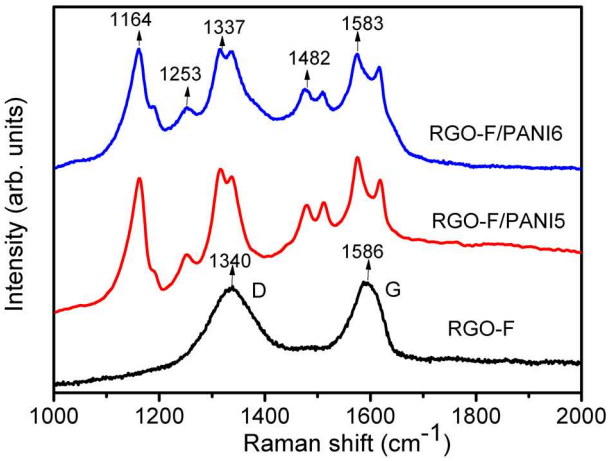

Figure 4. Raman spectra of RGO-F, RGO-F/PANI5 and RGO-F/PANI6 composites.

XPS studies were employed to monitor the progress of the characteristic binding energy of the C 1s and N 1s peaks corresponding to each functional group on the RGO-F and RGO-F/PANI composites. As shown in Figure 5A, the peak at 284.8, 400.6 and 532.9 eV can be assigned to C 1s, N 1s and O 1s, respectively.[40] Nitrogen elements are introduced to RGO-F networks as indicated by the N 1s signal. From these XPS survey spectra, it is found that the N content in RGO-F/PANI5 and RGO-F/PANI6 are 1.58 atom% and 3.64 atom%, respectively (Table S1). The high resolution XPS C 1s spectrum of RGO-F is given in Figure 5B. The C 1s XPS spectrum is deconvoluted into three peaks, which are related to C=C (284.3 eV), C-C (285.3 eV), C-O (286.4 eV), C=O (287.4 eV), O-C=O (289.0 eV).[40-41] The peak at 286.4 eV of RGO-F/PANI5 is attributed to C-N configurations because of the doping of nitrogen atoms, as shown in Figure 5C. In agreement with the above results, high-resolution N 1s spectra of RGO-F/PANI5 further supply detailed structural information of PANI grown on the 3D porous RGO-F. Three peaks in Figure 5D indicate that most of the nitrogen atoms in PANI are in the form of benzenoid amine (–NH–) centered at 399.5 eV with additional small peaks, including quinoid imine (-N=) (398.2 eV) and positively charged nitrogen atoms (-NH^+=) (401.0 eV). [40, 42-43]

3.2. Electrochemical performance

The conductivity of well-defined and interconnected 3D RGO-F is measured to be 1600 S m^{-1} based on a four-probe method. This remarkable conductivity and its mechanical stability enable RGO-F to be directly as electrodes to fabricate supercapacitors without adding polymer binders and conducting additives. A supercapacitor was assembled from two pieces of three dimensional RGO-F/PANI5 composite electrodes, with each a mass loading of 0.65 mg cm^{-2}. The assembled devices was lightweight (10±0.5 mg), thin (1±0.2 mm), and highly flexible. Figure 6 show the as-fabricated SCs based on RGO-F/PANI5 electrodes has an excellent flexibility and good mechanical properties.

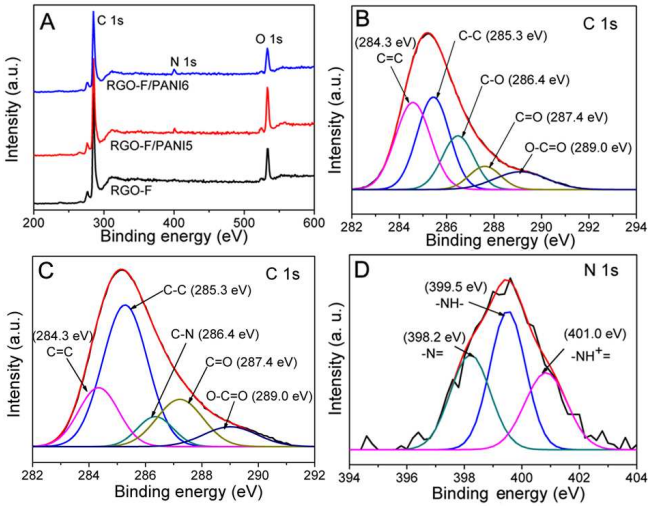

Figure 5. (A) XPS survey spectra of RGO-F, RGO-F/PANI5 and RGO-F/PANI6 composites. (B) C 1s high resolution XPS spectra of RGO-F, (C) C 1s and (D) N 1s XPS spectra of the RGO-F/PANI5.

Figure 7A shows the cyclic voltammograms (CVs) for bare 3D RGO-F at a scan rate ranging from 10 to 500 mV s^{-1} in a two-electrode system. The nearly symmetrical rectangular CV curves manifest the ideal double-layer capacitive behavior. The shape of CV curve remains even at a high scan rate of 500 mV s^{-1}, implying a low contact resistance. Therefore, we can deduce that the 3D RGO-F formed from NF can be used as freestanding flexible electrodes, which is an attractive scaffold for PANI nanowire arrays.

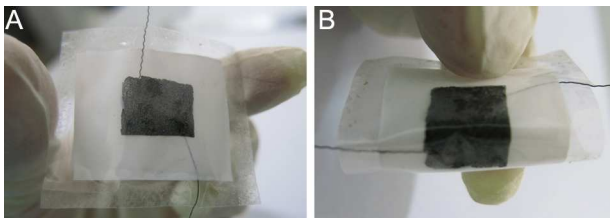

Figure 6. Digital photograph of flexible superacpacitors based on RGO-F/PANI5.

The electrochemical properties of RGO-F/PANI composites were evaluated using a symmetric two-electrode system in 1 M H_2SO_4 aqueous solution. Figure 7B shows that the CV curves area of flexible RGO-F/PANI supercapacitor is dramatically enhanced by the introduction of PANI nanowires onto 3D RGO-F. Two pairs of redox peaks in the CV curves of RGO-F/PANI supercapacitor correspond to the leucoemeraldine/emeraldine and emeraldine/pernigraniline transitions of PANI.[21, 44] The current density increases with the rising PANI concentration, suggesting that the capacitance is improved by incorporating pseudocapacitive materials with the 3D porous structure. It also can be confirmed from the triangle shape of the charge/discharge curves with a small potential drop and an increase discharge time in Figure 7C. The gravimetric capacitance of the devices at various current densities was calculated from the discharge curves, as shown in Figure 7D. The specific capacitance of 3D RGO-F, RGO-F/PANI5 and RGO-F/PANI6 supercapacitors is 90, 725 and 790 F g^{-1} at a current density of 1 A g^{-1}, respectively. The value of RGO-F/PANI5 supercapacitor exceeds those in previous reported systems based on graphene/PANI (233-763 F g

$^{-1}$),[26, 42-43, 45-46] owing to the small diameters (~ 50 nm) and short length (~150 nm) of PANI nanowires. The formation of small size nanowires increases the exposed surface area of PANI to the electrolyte ions and results in the enhancement of the specific capacitance. Moreover, the 3D porous RGO-F can be served as current collectors and form a conductive network under the PANI layer. Besides, the RGO-F/PANI5 supercapacitor possesses a superior rate capability. When the current density increased to 10 A g^{-1}, the specific capacitance is 598 F g^{-1}, maintaining 82% of that at 1 A g^{-1}. A press was used in a control experiment and 15 MPa force applied, the RGO/PANI electrode then had a thickness of about 60 ± 2 μm. Thus, the volumetric capacitance (C_{vol}) of RGO/PANI5 and RGO/PANI6 composite was calculated to be 174 ± 8 F cm^{-3} and 205.4 ± 8 F cm^{-3}, which is higher than carbide derived carbons and commercial carbons. [47-48]

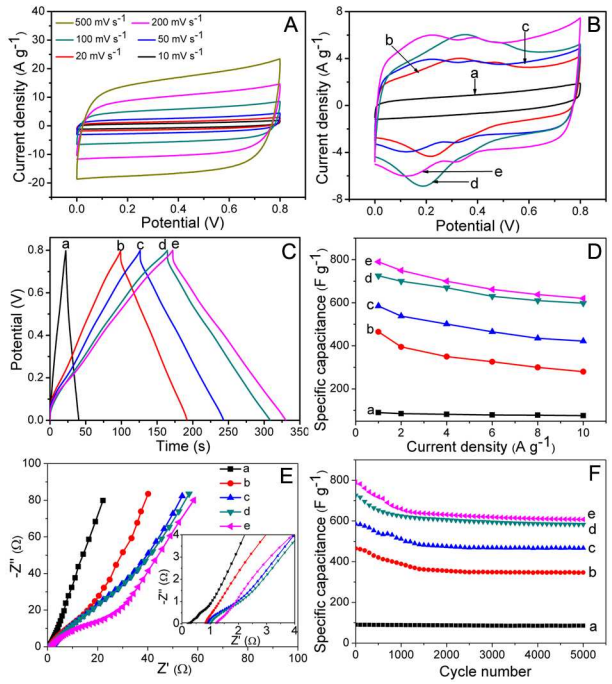

Figure 7. Electrochemical characteristics of flexible supercapacitors based on (a) RGO-F, (b) RGO-F/PANI3, (c) RGO-F/PANI4, (d) RGO-F/PANI5 and (e) RGO-F/PANI6 electrodes in 1 M H_2SO_4 aqueous solution. (A) CV curves of RGO-F at the scan rate range of 10 - 500 mV s^{-1}. (B) CV curves at a scan rate of 10 mV s^{-1}. (C) Galvanostatic charge/discharge measurements at 1 A g^{-1}. (D) Specific capacitance plots at different current densities from 1 A g^{-1} to 10 A g^{-1}. (E) Nyquist plots at a frequency range from 0.01 Hz to 10^5 Hz. The inset shows the high frequency part of the Nyquist plots. (F) Cycling stability at a current density of 1 A g^{-1}.

The Nyquist plots of 3D RGO-F and RGO-F/PANI supercapacitors obtained using electrochemical impedance spectroscopy (EIS) in the frequency range from 0.01 Hz to 10^5 Hz at open circuit potential are shown in Figure 7E with an expanded view of the high-frequency region in the inset. RGO-F/PANI supercapacitors show very low equivalent series resistance values (0.84 - 1.16 Ω), suggesting that the RGO-F/PANI devices have a very small resistance with a rapid ion response at high-frequency ranges even with a high loading of PANI nanowires. 3D flexible RGO-F/PANI supercapacitors show a nearly ideally capacitive behavior due to the fast and reversible redox reaction of PANI nanowire arrays. The small resistances are also confirmed by observing the small voltage drops at the beginning of discharge curves in Figure 6C.

The stability of the 3D RGO-F and RGO-F/PANI supercapacitors was evaluated using a long-term galvanostatic charge/discharge process (Figure 7F). The 3D RGO-F exhibits an excellent stability over the entire cycle range and remains 95% of initial capacitance. The RGO-F/PANI5 composite with highly ordered PANI nanowires arrays exhibits a superior stability by decreasing 17% of its specific capacitance after 5000 cycles at a current density of 1 A g^{-1}, while the RGO/PANI6 remains 80% of the initial specific capacitance after 5000 cycles. In the first 1000 cycles, a small decrease in the specific capacitance can be seen, while the value remains almost constant afterwards. The strong π–π interaction between the RGO-F and PANI nanowires effectively improves the long-term stability. The 3D RGO-F as a support skeleton allow the uniform deposition of PANI nanowires on their surfaces, which enhance the mechanical strength of hybrid materials. In addition, the decrease of the specific capacitance can be attributed to the swelling, shrinkage and overoxidation of the PANI nanowires leading to deterioration of the polymeric conductivity and charge storage capability during the charge/discharge process.[49] Then, the interaction force between RGO-F and PANI nanowires remained unchanged, indicating that the transfer ability of charges would keep fairly constant.[50] The ESR values of RGO-F/PANI5 electrode (from 10 to 8.5 ohms) has a small drop in the first 1000 cycles with only subtle changes for the remaining cycles (Figure S4). Furthermore, during the long cycling process, the coulombic efficiency exhibits retention of as high as 99% due to the small size PANI nanowires structure which ensures an efficient mass transportation (Figure S4). Thus, RGO-F/PANI composites with high order structure show superior electrochemical performances than pure PANI and RGO-F.

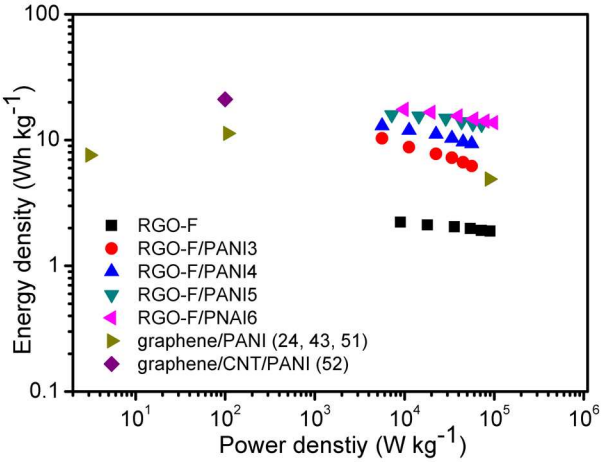

Figure 8. Ragone plot of RGO-F and RGO-F/PANI composites electrodes and and others using similar systems reported in the literature.

Figure 8 shows the Ragone plots of RGO-F supercapacitor and RGO-F/PANI supercapacitor. Obviously, the as-fabricated symmetric RGO-F/PANI supercapacitors shows much higher energy and power densities than that of RGO-F supercapacitor. The RGO-F supercapacitor exhibits a maximal energy density of 2.2 Wh kg^{-1} and power density of 90.3 kW kg^{-1}. RGO-F/PANI6

supercapacitor exhibits a maximum energy density and power density of 17.6 Wh kg $^{-1}$ and 98 kW kg $^{-1}$, which is higher than that of RGO-F/PANI5 supercapacitor (15.9 Wh kg $^{-1}$ and 72 kW kg $^{-1}$). These values are higher than that of reported symmetric supercapacitors, such as graphene/PANI nanofibers (4.9 Wh kg $^{-1}$, 8.8 kW kg $^{-1}$),[24] graphene/mesoporous PANI (11.3 Wh kg $^{-1}$, 106.7 W kg $^{-1}$),[51] and graphene nanoribbon/PANI (7.6 Wh kg $^{-1}$, 3.1 kW kg $^{-1}$).[43] It is also comparble to graphene/MWCNT/PANI electrodes (21.1 Wh kg $^{-1}$, 100 W kg $^{-1}$),[52] which is a potential electrode in the next generation supercapactiors.

The outstanding performance of the RGO-F/PANI5 symmetric supercapacitor can be ascribed to the following factors. First, the high conductivity and porous structure of the flexible 3D RGO-F could serve as superhighways for electron transfer and easy access for electrolyte ions to the electrode surfaces, providing both enhanced energy storage and good rate capability. Second, the PANI nanowire arrays with nanometer size are uniformly deposited on the network of 3D RGO-F through π–π interaction, which reduces the diffusion length of ions in PANI phase during rapid redox reaction, and ensure a high utilization of electrode materials leading to a high energy density of the symmetric supercapacitors. Third, hierarchically porous structure of RGO-F/PANI increases the active surface area and full accessibility for the electrolyte to the PANI nanowires, hence improving the electrochemical performance of electrodes. In addition, 3D porous RGO-F needs no binders or conducting additives, which decrease extra contact resistance or weight.

4. CONCLUSIONS

In summary, we have successfully built symmetric supercapacitors with both high power and high energy density using 3D RGO-F/PANI composite electrodes. PANI nanowire arrays are vertically grown on the surface of 3D flexible RGO-F foam network. The RGO-F/PANI6 supercapacitor shows high specific capacitance (790 F g $^{-1}$ at 1 A g $^{-1}$) and volumetric capacitance (205.4 F cm $^{-3}$), and exhibits maximum energy density and power density of 17.6 Wh kg $^{-1}$ and 98 kW kg $^{-1}$, which are about eight time higher than that of RGO-F supercapacitor (2.2 Wh kg $^{-1}$). Moreover, the symmetric supercapacitor exhibits excellent cycle stability with 80% capacitance retention after 5000 cycles, due to the synergetic effects of both the PANI and porous RGO-F foam contribute to the enhanced cycling stability. Therefore, the 3D lightweight and freestanding symmetric supercapacitor is a promising candidate in the application of high-performance energy storage systems.

ACKNOWLEDGEMENTS

Financial support of this work is provided by SRFDP (20110075110009), SRFDP (20130075120018), 111 Project (111-2-04) and Innovation Funds for PhD Students of Donghua University (12D10630).

Notes and references

[a] *State Key Laboratory for Modification of Chemical Fibers and Polymer Materials, College of Materials Science and Engineering, Donghua University, Shanghai 201620, China. Telephone/Fax: 0086-21-67792854; E-mail: qhzhang@dhu.edu.cn.*

† Electronic Supplementary Information (ESI) available: [AFM image of GO. The FTIR spectra of RGO-F, PANI, RGO-F/PANI5 and RGO-F/PANI6 composites. The Raman spectrum of GO foam. The plots of Coulombic efficiency (left axis) and ESR (right axis) for RGO-F/PANI5. XPS data of RGO-F and RGO-F/PANI compsoites]. See DOI: 10.1039/b000000x/.

1. H. Nishide and K. Oyaizu, *Science,* 2008, **319**, 737-738.
2. L. Nyholm, G. Nyström, A. Mihranyan and M. Strømme, *Adv. Mater.,* 2011, **23**, 3751-3769.
3. X. Lu and Y. Xia, *Nat. Nanotechnol.,* 2006, 163-164.
4. L. L. Zhang and X. S. Zhao, *Chem. Soc. Rev.,* 2009, **38**, 2520-2531.
5. P. Simon and Y. Gogotsi, *Nat. Mater.,* 2008, **7**, 845-854.
6. B. E. Conway, *Electrochemical supercapacitors: scientific fundamentals and technological applications*. Plenum: New York: 1999.
7. F. Beguin and E. Frackowiak, *Supercapacitors*. Weinheim: Wiley: 2013.
8. F. Beguin, V. Presser, A. Balducci and E. Frackowiak, *Adv. Mater.,* 2014, **26**, 2219-2251, 2283.
9. Y. He, W. Chen, X. Li, Z. Zhang, J. Fu, C. Zhao and E. Xie, *ACS Nano,* 2012, **7**, 174-182.
10. J. J. Yoo, K. Balakrishnan, J. Huang, V. Meunier, B. G. Sumpter, A. Srivastava, M. Conway, A. L. Mohana Reddy, J. Yu, R. Vajtai and P. M. Ajayan, *Nano Lett.,* 2011, **11**, 1423-1427.
11. Y. Zhu, S. Murali, M. D. Stoller, K. J. Ganesh, W. Cai, P. J. Ferreira, A. Pirkle, R. M. Wallace, K. A. Cychosz, M. Thommes, D. Su, E. A. Stach and R. S. Ruoff, *Science,* 2011, **332**, 1537-1541.
12. W. Gao, N. Singh, L. Song, Z. Liu, A. L. M. Reddy, L. Ci, R. Vajtai, Q. Zhang, B. Wei and P. M. Ajayan, *Nat. Nanotechnol.,* 2011, **6**, 496-500.
13. Y. Xu, K. Sheng, C. Li and G. Shi, *ACS Nano,* 2010, **4**, 4324-4330.
14. J. Chen, K. Sheng, P. Luo, C. Li and G. Shi, *Adv. Mater.,* 2012, **24**, 4569-4573.
15. B. G. Choi, M. Yang, W. H. Hong, J. W. Choi and Y. S. Huh, *ACS Nano,* 2012, **6**, 4020-4028.
16. Z. Chen, W. Ren, L. Gao, B. Liu, S. Pei and H. M. Cheng, *Nat. Mater.,* 2011, **10**, 424-428.
17. J. Ji, L. L. Zhang, H. Ji, Y. Li, X. Zhao, X. Bai, X. Fan, F. Zhang and R. S. Ruoff, *ACS Nano,* 2013, **7**, 6237-6243.
18. X.-C. Dong, H. Xu, X.-W. Wang, Y.-X. Huang, M. B. Chan-Park, H. Zhang, L.-H. Wang, W. Huang and P. Chen, *ACS Nano,* 2012, **6**, 3206-3213.
19. X. Dong, J. Wang, J. Wang, M. B. Chan-Park, X. Li, L. Wang, W. Huang and P. Chen, *Mater. Chem. Phys.,* 2012, **134**, 576-580.
20. P. Yu, Y. Li, X. Zhao, L. Wu and Q. Zhang, *Synthetic. Met.,* 2013, **185–186**, 89-95.
21. Y. Li, X. Zhao, P. Yu and Q. Zhang, *Langmuir.,* 2012, **29**, 493-500.
22. Y. Li, Q. Zhang, X. Zhao, P. Yu, L. Wu and D. Chen, *J. Mater. Chem.,* 2012, **22**, 1884-1892.
23. C. C. Hu and C. H. Chu, *J. Electroanal. Chem.,* 2001, **503**, 105-116.
24. P. J. Hung, K. Chang, Y. F. Lee, C. C. Hu and K. M. Lin, *Electrochim. Acta,* 2010, **55**, 6015-6021.
25. Z. F. Li, H. Zhang, Q. Liu, L. Sun, L. Stanciu and J. Xie, *ACS Appl. Mater. Interfaces,* 2013, **5**, 2685-2691.
26. D. W. Wang, F. Li, J. Zhao, W. Ren, Z. G. Chen, J. Tan, Z. S. Wu, I. Gentle, G. Q. Lu and H. M. Cheng, *ACS Nano,* 2009, **3**, 1745-1752.
27. Q. Wu, Y. Xu, Z. Yao, A. Liu and G. Shi, *ACS Nano,* 2010, **4**, 1963-1970.

28. J. Zhang and X. S. Zhao, *J. Physic. Chem. C,* 2012, **116**, 5420-5426.
29. N. A. Kumar, H.-J. Choi, Y. R. Shin, D. W. Chang, L. Dai and J.-B. Baek, *ACS Nano,* 2012, **6**, 1715-1723.
30. X. Zhao, Q. Zhang, D. Chen and P. Lu, *Macromolecules.,* 2010, **43**, 2357-2363.
31. X. Zhao, Q. Zhang, Y. Hao, Y. Li, Y. Fang and D. Chen, *Macromolecules.,* 2010, **43**, 9411-9416.
32. P. Yu, Y. Li, X. Yu, X. Zhao, L. Wu and Q. Zhang, *Langmuir.,* 2013, **29**, 12051-12058.
33. D. A. Dikin, S. Stankovich, E. J. Zimney, R. D. Piner, G. H. B. Dommett, G. Evmenenko, S. T. Nguyen and R. S. Ruoff, *Nature,* 2007, **448**, 457-460.
34. C. Chen, Q. H. Yang, Y. Yang, W. Lv, Y. Wen, P. X. Hou, M. Wang and H. M. Cheng, *Adv. Mater.,* 2009, **21**, 3007-3011.
35. Y. Xue, D. Yu, L. Dai, R. Wang, D. Li, A. Roy, F. Lu, H. Chen, Y. Liu and J. Qu, *Phys. Chem. Chem. Phys.,* 2013, **15**, 12220-12226.
36. D. C. Elias, R. R. Nair, T. M. G. Mohiuddin, S. V. Morozov, P. Blake, M. P. Halsall, A. C. Ferrari, D. W. Boukhvalov, M. I. Katsnelson, A. K. Geim and K. S. Novoselov, *Science,* 2009, **323**, 610-613.
37. S. Niyogi, E. Bekyarova, M. E. Itkis, H. Zhang, K. Shepperd, J. Hicks, M. Sprinkle, C. Berger, C. N. Lau, W. A. deHeer, E. H. Conrad and R. C. Haddon, *Nano Lett,* 2010, **10**, 4061-4066.
38. H. Fan, H. Wang, N. Zhao, X. Zhang and J. Xu, *J. Mater. Chem.,* 2012, **22**, 2774-2780.
39. X. Yan, Z. Tai, J. Chen and Q. Xue, *Nanoscale,* 2011, **3**, 212-216.
40. Z. Gao, W. Yang, J. Wang, H. Yan, Y. Yao, J. Ma, B. Wang, M. Zhang and L. Liu, *Electrochim. Acta,* 2013, **91**, 185-194.
41. X. Y. Chen, C. Chen, Z. J. Zhang, D. H. Xie, X. Denga and J. W. Liu, *J. Power Sources,* 2013, **230**, 50-58.
42. T. Lee, T. Yun, B. Park, B. Sharma, H. K. Song and B. S. Kim, *J. Mater. Chem.,* 2012, **22**, 21092-21099.
43. L. Li, A. R. Raji, H. Fei, Y. Yang, E. L. Samuel and J. M. Tour, *ACS Appl. Mater. Interfaces,* 2013, **5**, 6622-6627.
44. Y. Li, X. Zhao, Q. Xu, Q. Zhang and D. Chen, *Langmuir.,* 2011, **27**, 6458-6463.
45. L. Mao, K. Zhang, H. S. O. Chan and J. Wu, *J. Mater. Chem.,* 2012, **22**, 80-85.
46. H. P. Cong, X. C. Ren, P. Wang and S. H. Yu, *Energy Environ. Sci.,* 2013, **6**, 1185-1191.
47. D. Weingarth, D. Cericola, F. C. F. Mornaghini, T. Hucke and R. Kötz, *J. Power Sources,* 2014, **266**, 475-480.
48. J. Chmiola, G. Yushin, R. Dash and Y. Gogotsi, *J. Power Sources,* 2006, **158**, 765-772.
49. C. Meng, C. Liu, L. Chen, C. Hu and S. Fan, *Nano Lett.,* 2010, **10**, 4025-4031.
50. J. Li, H. Xie, Y. Li, J. Liu and Z. Li, *J. Power Sources,* 2011, **196**, 10775-10781.
51. Q. Wang, J. Yan, Z. Fan, T. Wei, M. Zhang and X. Jing, *J. Power Sources,* 2014, **247**, 197-203.
52. J. Shen, C. Yang, X. Li and G. Wang, *ACS Appl. Mater. Interfaces,* 2013, **5**, 8467-8476.